Research Square

Preprints are preliminary reports that have not undergone peer review.
They should not be considered conclusive, used to inform clinical practice,
or referenced by the media as validated information.

Isoliensinine Sensitizes Gastric Cancer Cells to FDX1-Mediated Cuproptosis by Targeting Mitochondria

Siyi Zhang
Affiliated Hospital of Qingdao University
Yuanyuan Fang
Affiliated Hospital of Qingdao University
Kun Chi
Qingdao Municipal Hospital
Jia lin Song
Affiliated Hospital of Qingdao University
Yangyang Lu
Affiliated Hospital of Qingdao University
Shasha Wang
Affiliated Hospital of Qingdao University
Wei wei Qi
Affiliated Hospital of Qingdao University
Wensheng Qiu
wsqiuqdfy@qdu.edu.cn

Affiliated Hospital of Qingdao University

Research Article

Keywords: Gastric cancer, Isoliensinine, Mitochondrial metabolism, Cuproptosis, FDX1

Posted Date: September 16th, 2026

DOI: https://doi.org/10.21203/rs.3.rs-10907028/v1

License: This work is licensed under a Creative Commons Attribution 4.0 International License.
Read Full License

Additional Declarations: No competing interests reported.

Abstract

Background

Gastric cancer, a prevalent and highly lethal malignancy, presents significant clinical challenges due to chemotherapy resistance and limited efficacy of targeted therapies. Natural products such as isoliensinine (ISO), a low-toxicity phenolic dibenzylisoquinoline alkaloid with demonstrated anti-tumor properties, represent promising therapeutic candidates. However, the effects of ISO on gastric cancer and its potential for synergistic therapeutic combinations remain poorly defined.

Methods

The *in vitro* effects of ISO on gastric cancer cell proliferation, migration, cell cycle, and apoptosis were evaluated using MTT assays, wound healing assays, colony formation assays, and Western blot. The inhibitory effect of ISO on gastric cancer *in vivo* was validated using a *BALB/c* nude mouse model. Transcriptomic sequencing and Western blot were employed to verify the associated signaling pathways, while Western blot combined with fluorescence staining assessed mitochondrial function and oxidative stress levels. The combined anti-tumor effects of ISO with cisplatin or the cuproptosis inducer Elesclomol-Cu (ES-Cu) were determined using MTT assays, wound healing assays, colony formation assays, Western blot, and immunofluorescence. Molecular docking, molecular dynamics simulations, and siRNA technology were utilized to determine the critical role of FDX1 in the synergistic effect of ISO with cuproptosis.

Results

ISO dose-dependently inhibited gastric cancer cell viability. It also induced G1-phase cell cycle arrest and triggered mitochondrial apoptosis through ROS accumulation and activation of the JNK/p38 MAPK pathway. In vivo, ISO significantly suppressed tumor growth in mouse models without observable toxicity. Crucially, ISO synergized with cuproptosis inducers (ES-Cu), amplifying DLAT oligomerization and ROS generation. Mechanistically, this synergy specifically depended on targeting FDX1—a key regulator of cuproptosis—as FDX1 knockdown abolished the combinatorial effect. Moreover,The combination of ISO with the chemotherapy drug cisplatin enhanced the inhibition of tumor cell growth.

Conclusion

Our findings confirm ISO inhibits gastric cancer progression by inducing mitochondrial apoptosis and G1-phase cell cycle arrest. Its synergistic interaction with cuproptosis inducers is mechanistically dependent on FDX1 targeting, which intensifies DLAT aggregation and oxidative stress. These findings

identify ISO, particularly in combination with cuproptosis induction, as a novel combinatorial strategy against gastric cancer.

1. Introduction

Gastric cancer, a malignant tumor with a continuously rising global incidence rate, presents significant treatment challenges[1–2]. According to the latest statistics from the International Agency for Research on Cancer, gastric cancer accounts for over 1.1 million new cases every year, ranking fourth among cancer-related causes of death, with a five-year survival rate of less than 10% for patients with advanced disease[3–4]. This dire situation is closely linked to the limitations of current treatment methods. Platinum-based chemotherapy drugs, represented by cisplatin, exert broad-spectrum anti-tumor effects by inducing DNA cross-linking damage and activating p53-dependent apoptosis pathways[5]. However, clinical data indicate that over 60% of gastric cancer patients develop acquired resistance within 12 months after receiving platinum-based treatment, leading to rapid disease progression[6]. In addition, the high heterogeneity of gastric cancer leads to slow progress in targeted therapy. Except for HER2-positive patients who can benefit from trastuzumab[7], inhibitors targeting pathways such as VEGFR and EGFR demonstrate low clinical response rates and frequent lead to secondary resistance mutations[8–9]. This clinical dilemma urgently requires breakthroughs from a deeper understanding of cell death mechanisms.

Natural products play an essential role in anti-tumor research due to their structural diversity and multi-target mechanisms of action[10]. Currently, over 60% of anti-cancer drugs are derived from plants, marine organisms, or microorganisms, including classic drugs such as paclitaxel, vincristine, and camptothecin[11–12]. In recent years, the combined application of natural products has demonstrated significant potential in the field of oncology. Through multi-mechanism collaboration, this approach has gradually become a key strategy for enhancing therapeutic efficacy. Previous studies have shown that the combination of natural products and chemotherapy drugs can not only enhance the therapeutic activity but also reduce their chemotherapy-induced toxicity[13–14]. At the same time, natural products can be integrated with different types of cell death mechanisms to exert their anti-cancer effects. For instance, quercetin simultaneously inhibits the Wnt3a/β-catenin and Akt/NF-κB signaling pathways to affect the expression of key DNA repair enzyme MGMT, thereby promoting glioblastoma apoptosis[15]. Similarly, Hesperidin degrades SLC7A11 via the ubiquitin proteasome pathway, indirectly inhibiting GPX4 activity and inducing ferroptosis in liver cancer cells[16]. Phthalate lactone (PoD) also inhibits the activity of PRDX1, leading to intracellular copper ion accumulation and activating the Caspase-dependent apoptosis pathway, establishing a dual anti-cancer mechanism[17].

ISO is a bisbenzylisoquinoline alkaloid extracted from the seed embryos of lotus plants in the Nymphaeaceae family. It has attracted significant interest due to its antioxidant, anti-inflammatory, and anticancer properties[18–19]. The anticancer efficacy of isoleucine involves synergistic regulation across multiple pathways. In triple-negative breast cancer, ISO significantly inhibits the proliferation of tumor

cells by inducing the accumulation of reactive oxygen species and activating the p38 MAPK and JNK signaling pathways[20]. In cervical cancer, ISO inhibits AKT phosphorylation, upregulates the cycle regulatory protein p21, leading to cell cycle arrest in the G0/G1 phase, and synergistically enhances the anti-cancer effect with AKT inhibitors[21]. In addition, ISO can induce cancer cell apoptosis while exhibiting reduced toxicity to normal liver cells in liver cancer models by inhibiting the activity of key transcription factor p65 in the NF-κB signaling pathway, downregulating its downstream anti-apoptotic genes[22]. However, the therapeutic efficacy and potential for the combination use of ISO in gastric cancer remain unclear. This study aimed to demonstrate the effects of ISO on the proliferation, migration, and apoptosis of gastric cancer cells, and to validate its safety *in vivo*. Similarly, we demonstrated that ISO induced mitochondrial dysfunction in gastric cancer cells and altered the levels of ROS. Besides, ISO was combined with cuproptosis, a novel therapeutic strategy, to target tumor cells, and its specific mechanisms were explored. For potential clinical applications, ISO was tested in combination with the chemotherapeutic drug cisplatin to enhance cancer cell cytotoxicity.

2. Materials and Methods

2.1. Reagents and materials

Isoliensinine (ISO, T5S 1103, Target Mol), dimethyl sulfoxide (DMSO, HY-Y0320, MCE), 3- (4,5-dimethylthiazole-2) -2,5-diphenyltetrazolium bromide (MTT; M158055, Aladdin), crystal violet (C110703, Aladdin), iodopropydine (PI; P4170, Sigma Aldrich), 2 ', 7' - dichlorodihydrofluorescein diacetate (H2DCFDA; D6883, Sigma Aldrich), dihydroethidium (DHE; 37291, Sigma Aldrich), JC-1 mitochondrial membrane potential assay kit (40706ES60, Ye) asen Biotechnology), Elesclomol (ES; T6170, Targeted Mol), Copper(II) chloride dihydrate (307483, Sigma-Aldrich); DAPI staining solution (5mg/ml) (40728ES03, Yisheng Biotechnology) Hieff Trans ® SiRNA/miRNA in vitro transfection reagent (40806ES, Yisheng Biotechnology), goat anti rabbit IgG (H + L) (FITC conjugated) (E-AB-1014, Elabscience Biotechnology Co., Ltd.). Cle-caspase9 polyclonal antibody (9505T, CST), Bad polyclonal antibody (A19595), Bax polyclonal antibody (A19684), Bcl-2 polyclonal antibody (A200777), Cyclin D1 polyclonal antibody (A19038), CDK2 polyclonal antibody (A0094) were purchased from ABclonal Technology Co., Ltd. P21 polyclonal antibody (25614-1-AP), P27 polyclonal antibody (10355-1-AP), p-JNK polyclonal antibody (80024-1-RR), JNK polyclonal antibody (51151-1-AP), p-P38 polyclonal antibody (28796-1-AP), P38 polyclonal antibody Antibodies (14064-1-AP), DLAT polyclonal antibodies (13426-1-AP), ETFDH polyclonal antibodies (11109-1-AP), LIAS polyclonal antibodies (11577-1-AP), and FDX1 polyclonal antibodies (12592-1-AP) were all purchased from Sanying Technology Co., Ltd

2.2. Cell culture

Human gastric mucosal cell line (GES-1) and gastric cancer cell lines (AGS, HGC27 and MFC) were purchased from the cell bank of the Typical Culture Preservation Center of the Chinese Academy of Sciences (Shanghai, China). All cells were obtained through legal channels and subjected to short tandem repeat (STR) identification. For routine experiments, these cell lines were cultured in Procell Life

Science & Technology Co., Ltd. (RPMI) -1640 medium supplemented with 10% fetal bovine serum (FBS; Life iLab, China), 100 U/mL penicillin, and 100 μg/mL streptomycin at 37°C and 5% CO_2.

2.3. Cell viability assay

Cell viability was evaluated using the MTT assay after treatment with ISO alone or in combination with CIS or ES-Cu. After drug treatment, the culture medium was aspirated, and MTT working solution (0.5 mg/ml) was injected into the cells, which were then incubated in a CO_2 incubator for 3–6 hours. After incubation, the obtained formazan crystals were dissolved in DMSO and the absorbance was measured at 490nm using a microplate reader (BioTek, USA). The cell viability was calculated using the formula: treatment group cell viability (%)=A490/control group A490.

2.4. Colony-forming assay

A colony formation assay was performed using a 6-well plate, with 1000 cells seeded in each well. Cells were then treated with ISO alone or in combination with CIS or ES-Cu. After processing, cells were cultured under controlled conditions in a cell culture incubator to promote stable. After incubating for 10–14 days, the cells were fixed with 4% paraformaldehyde and stained with crystal violet and photographed.

2.5. Migration assays

Cells were seeded in 24-well plates, and stable cell cultures were maintained. When the cell density exceeded 90% of the area of each well, a wound was created on the cell surface using a 200 μL. After washing the floating cells with phosphate-buffered saline (PBS), the adherent cells were grown in culture medium for 4 h. Wound width was measured using a microscope (Nikon, Japan) after 48 h of drug treatment and incubation, and the data were analyzed using ImageJ software.

2.6. Cell viability and cytotoxicity testing

Dead cells were stained with propidium iodide (PI; P4170, Sigma Aldrich) and exhibited red fluorescence. After 48 hours of drug treatment, the working solution, prepared according to the kit instructions, was added to the cells. The cells were then placed in a CO_2 incubator and incubated in the dark for 30 minutes. After incubation, the staining effect was observed under an inverted fluorescence microscope (Nikon, Japan).

2.7. Animal experiments

Beijing Weitonglihua Experimental Animal Technology Co., Ltd. provides female 4-week-old BALB/c nude mice, which are housed in the Experimental Animal Center of Qingdao University Biomedical Center. Before the experiment, mice were first acclimated to an environment without specific pathogens, with constant temperature, humidity, and appropriate lighting conditions for one week. All programs have been approved by the Ethics Committee of Qingdao University Affiliated Hospital and comply with the ethical treatment guidelines for experimental animals. MFC cells (1.5×10^5) were injected subcutaneously into the back of BALB/c nude mice at a dose of 100 μ L. After 2 days of growth, the mice

were divided into three groups: control group, low concentration ISO group (5 mg/Kg), and high concentration ISO group (10mg/Kg), with 4 mice in each group. Administer via intraperitoneal injection every 2 days, measure the body weight and tumor volume of mice before each administration (tumor volume (mm^3) =length ×width ^{2} ×0.5). After 2 weeks, euthanize the mice, collect tumor tissue, weigh, photograph, and measure its size. Take the mouse heart, liver, spleen, and kidneys, fix them with paraformaldehyde, and hand them over to Wuhan Sevier Biotechnology Co., Ltd. for histopathological examination.

2.8. RNA sequencing

AGS cells were cultured overnight in a 10 mm cell culture dish. To obtain total RNA, ISO (30 μ mol/l) treatment was applied and the correct cell density was waited for 48 hours. There is a total RNA exceeding 20 ng/ul. Afterwards, Shanghai Jingfang Biotechnology Co., Ltd. will use the obtained RNA for RNA sequencing. The RNA sequencing process includes three steps: mRNA capture, high-throughput sequencing library construction, and machine sequencing. Usually, oligo dT microbeads are used to collect RNA fragments with polyA tails and heated to generate high-throughput sequencing libraries. After quality inspection, the library was sequenced on the Illumina NovaSeq 6000 platform. We use DESeq2 to examine different fully expressed genes.

2.9. Mitochondrial membrane potential (MMP) assay

Changes in mitochondrial membrane potential were detected through the transition of JC-1 from red to green fluorescence. A JC-1 mitochondrial membrane potential detection kit (40706ES60, Yeasen Biotechnology) was used, and the JC-1 staining working solution was prepared according to the provided instructions. Following the cell experiment treatment, the staining working solution was added, and cells were incubated at 37 ºC for 30 minutes in a cell culture incubator. After incubation, the supernatant was aspirated, and the cells were washed twice with PBS. MMP changes were then immediately observed and detected under an inverted fluorescence microscope (Nikon, Japan).

2.10. Reactive oxygen species detection

H2DCFDA (DCF, 10 μmol/l)/DHE (10 μmol/l) dyes were prepared in RPMI 1640 medium without FBS. The cells were incubated in a 24-well plate for 24 hours before treatment with various drugs. At the end of the experiment, the dye was added to the cells and incubated for 45 minutes. The cells were washed twice with PBS and imaged using an inverted fluorescence microscope (Nikon, Japan).

2.11. siRNA transfection

Template interference RNA (siRNA) was transfected into GenePharma to synthesize the following target sequence siRNA: siFDX1.AGS (1.2 ×10^5cells/well) and HGC27 (1×10^5 cells/well) cells were cultured overnight in a 6-well plate. According to the manufacturer's instructions, Hieff Trans ® SiRNA/miRNA in vitro transfection reagent was used to transfect siRNA into gastric cancer cells, after which the experiment proceeded to the next step.

2.12. Molecular docking studies

The 3D structure of small molecules was downloaded in SDF format from the PubChem data. The optimized small molecules were imported into AutodockTools-1.5.6 for hydrogenation, charge calculation, and charge allocation. The protein structures were downloaded from the PDB protein database based on the provided PDB ID. POCASA 1.1 was used to predict protein binding sites, and AutoDock Vina 1.1.2 was employed for docking.

2.13. Molecular dynamics

The protein ligand complex obtained by molecular docking was analyzed using full atomic molecular dynamics simulation using GROMACS 2022.4 software. For the protein component, the TIP3P water model was employed, and an appropriate amount of sodium and chloride ions was added to neutralize the overall system charge. For each equilibrated system, molecular dynamics simulations were conducted at 300K for 100ns, resulting in a total of 10000 simulated trajectories. Key parameters such as root mean square deviation (RMSD), radius of gyration (Rg), and total number of hydrogen bonds between proteins and ligands were analyzed in depth using simulated trajectory files.

2.14. Immunofluorescence assay

After 48 hours of treatment with ISO combined with ES and Cu, AGS and HGC27 cells were fixed with 4% paraformaldehyde after staining with mitochondrial probes for 30 minutes. Then, cells were permeabilized with 0.2% Triton X-100 and blocked with 5% BSA to reduce non-specific antibody binding. Incubate the cells overnight with primary antibodies against DLAT. Detection was performed using a FITC-conjugated goat anti-rabbit IgG (H + L) secondary antibody. Finally, DAPI staining was used to observe the cell nucleus, and images were captured using a laser confocal microscope (Leica, Germany). All fluorescence images were captured using a confocal microscope (Leica, Germany).

2.15. Western blot

After the cells were treated with drugs in a 10cm dish for 48 hours, they were scraped off with a scraper. The cells were then lysed with IP buffer, and the supernatant was collected via centrifugation. Cell proteins (20 μg/sample) were separated using 10% SDS-PAGE and subsequently transferred to a PVDF membrane (10600023, Cytiva). The PVDF membrane was sealed with 5% skim milk for 1 hour, followed by an overnight incubation with the primary antibody at 4°C. The membrane was washed three times with washing buffer (10 minutes each wash), and then incubated with secondary antibody at 37°C for 1 hour. Finally, the membrane was washed with washing buffer three additional times (each for 10 minutes) before development.

2.16. Statistical analysis

Each experimental result is based on three independent repeated experiments (n = 3), and each statistical data is represented as mean ± SEM. Statistical analysis was conducted using GraphPad Prism 9.5.0 software, and one-way ANOVA and multiple comparisons were used to analyze inter group differences. A P value of < 0.05 was considered statistically significant (ns indicates $P > 0.05$, * $P < 0.05$, * * $P < 0.01$, * * $P < 0.001$, * * * * $P < 0.0001$).

3. Results

3.1. ISO inhibits gastric cancer cells *in vivo* and *in vitro*

Figure 1A illustrates the structure of ISO. The MTT assay was used to evaluate the cytotoxicity of ISO (0, 10, 15, 20, 30, and 40μmol/L) treatment on GES-1 cells at 24 or 48 hours. The results showed that ISO exhibited low toxicity, with no significant change in the viability of GES-1 cells after 24 or 48 hours of treatment at concentrations ranging from 0 to 30μmol/L (Fig. 1B). Subsequently, the cytotoxic effect of ISO on gastric cancer cells was evaluated at the same concentrations. The results showed that the viability of AGS, HGC27, and MFC cells decreased steadily in a dose and time-dependent manner compared to the control group (Fig. 1B). These findings suggest that ISO can selectively kill tumor cells. Further investigation into the mechanism of ISO action involved treating AGS, HGC27, and MFC cell lines with ISO for 48 hours, followed by PI staining to assess membrane integrity. Increased red luminescence intensity was observed in the highest ISO concentration group, indicating varying degrees of cell membrane and cellular damage (Fig. 1C). Similar results were obtained by crystal violet staining (Fig. 1D). Live AGS, HGC27, and MFC gastric cancer cells were assessed under a microscope and stained with crystal violet which revealed a gradual reduction in the number of viable cells with increasing ISO concentration and treatment duration, indicating a time- and concentration-dependent effect. Treated cells exhibited irregular, spherical, and bright shapes, consistent with the measured cell survival results (Fig. 1D). To further investigate the effect of ISO on the proliferation of AGS, HGC27, and MFC cells, cloning experiments were conducted, revealing that ISO treatment significantly reduced the formation of AGS, HGC27, and MFC cell colonies (Fig. 1E). The inhibitory effect of ISO on AGS and HGC27 cell migration was assessed using a cell scratch assay. During the 48-hour ISO treatment period, control group cells migrated extensively, nearly covering the entire scratch area. Conversely, an increase in ISO concentration resulted in a progressive decrease in the area of cell migration (Fig. 1F). Collectively, these findings indicated that ISO effectively inhibits the growth of AGS, HGC27, and MFC cells *in vitro*.

To evaluate the ability of ISO to inhibit tumor growth *in vivo*, MFC cells were used to examine the anti-tumor efficacy of ISO in BALB/c nude mice. MFC BALB/c nude mice were randomly divided into three groups when the tumor volume reached 50-100mm^3: control group, low concentration group (5 mg/kg), and high concentration group (10 mg/kg). Notably, no significant changes in weight were observed in all groups during the 4-week treatment period (Fig. 1H). Compared with the control group, both the low concentration and high concentration ISO groups showed inhibition of tumor volume growth (Fig. 1I-L). To further evaluate the efficacy and safety of ISO treatment, immunohistochemistry and hematoxylin and eosin (H&E) staining were used to assess tumor proliferation, cell apoptosis, and potential organ damage in mice. Immunohistochemistry showed that compared with the control group, the expression of Ki-67 (a pro-proliferative marker) in the ISO group was significantly reduced, indicating effective inhibition of tumor cell proliferation. Importantly, H&E staining of all major organs (heart, liver, spleen, and kidneys) showed no significant pathological changes (Fig. 1K), indicating that ISO yielded no toxic effects *in vivo*. Therefore, it can be concluded that ISO exhibits a high safety profile and can significantly inhibit the growth of transplanted tumors *in vivo*.

The above findings indicate that ISO exhibits significant inhibitory effects on gastric cancer cells in *in vivo* and *in vitro* experimental models, while also demonstrating high safety.

3.2. ISO induces mitochondrial-dependent apoptosis

To elucidate the molecular mechanisms underlying ISO's anti-tumor effects observed in vitro and in vivo, RNA sequencing was performed on AGS cells treated with 30μmol/L ISO ,with 3 replicates per group. The overall gene expression profile indicated that ISO could regulate gene translation in AGS cells. Compared with the control group, the ISO group produced 1980 differentially expressed genes (DEGs), of which 716 were upregulated and 1264 were downregulated (Fig. 2A-B). The lower number of upregulated genes compared to downregulated genes suggests that ISO significantly inhibits gene transcription in AGS cells, resulting in cellular functional arrest. Gene Ontology (GO) analysis was used to examine these differentially expressed genes. GO analysis showed that differentially expressed genes were significantly enriched in metabolic pathways and TCA cycle (Fig. 2D). KEGG analysis revealed that the differentially expressed genes were significantly enriched in DNA replication, cell cycle, p53 signaling pathways and MAPK signaling pathways (Fig. 2C).

Based on the RNA sequencing results, the expression of cell cycle-related proteins CyclinD1, CDK2, P21, and P27 was detected by Western blot. The results indicated that ISO upregulated cyclin-dependent kinase inhibitors p21 and p27, downregulated cyclin-dependent kinase CDK2, thereby preventing cells from entering the S phase from the G1 phase and causing cell cycle arrest in the G1 phase (Fig. 2H). Meanwhile, ISO inhibited the expression of cell cycle proteins, such as downregulating the expression of Cyclin D1, further hindering normal progression of the cell cycle.

Cell cycle arrest can lead to mitochondrial dysfunction. We first examined the mitochondrial membrane potential to determine whether ISO-induced cellular toxicity was associated with mitochondrial function and oxidative stress. The JC-1 method was used to determine the effects of ISO on AGS, HGC27, and MFC cells. Increased ISO concentrations led to increased JC-1 monomers (green fluorescence) and decreased JC-1 aggregates (red fluorescence), indicating mitochondrial depolarization, reduced mitochondrial membrane potential, and mitochondrial dysfunction (Fig. 2E). ROS are abundant oxidative intermediates generated during mitochondrial dysfunction. Subsequently, DCFH-DA staining and DHE staining were applied to detect the levels of intracellular ROS in gastric cancer cells treated with ISO. The results showed increased green fluorescence intensity (DCF) and red fluorescence intensity (DHE) in AGS, HGC27, and MFC cells exposed to ISO, indicating increased ROS levels in these three cell lines (Fig. 2F). Subsequently, Western blot analysis was conducted to detect changes in proteins related to apoptosis in gastric cancer cells AGS and HGC27. Notably, in AGS and HGC27 cells, the expression of anti-apoptotic protein Bcl-2 was downregulated, while the expression of apoptotic proteins Bax, Bad, and cleaved caspase-9/caspase-9 was significantly upregulated. These results collectively indicate that ISO activates mitochondrial-dependent pathways to induce gastric cancer cell death (Fig. 2G). In summary, ISO can induce mitochondrial apoptosis in gastric cancer cells by inducing oxidative stress.

Given that activation of the P38/JNK pathway can induce cell apoptosis, we speculate that ISO can also induce gastric cancer apoptosis through this pathway. Subsequently, the expression levels of MAPK pathway-related proteins p-P38/P38 and p-JNK/JNK were detected using Western blot. The results indicated that ISO treatment upregulated the expression of MAPK pathway-related proteins p-P38/P38 and p-JNK/JNK in a concentration-dependent manner. Compared to the control group, the expression levels of p-P38/P38 and p-JNK/JNK in cancer cells were elevated in the experimental groups (10, 20, 30μmol/L) (Fig. 2I). These results preliminarily suggest that ISO can inhibit the activity of cancer cells by affecting the p38/JNK pathway, although further verification is warranted.

3.3. ISO synergizes with ES-Cu to induce cuproptosis in gastric cancer cells

Cuproptosis—a novel copper-dependent mitochondrial cell death pathway driven by DLAT oligomerization and iron-sulfur cluster loss—represents a promising therapeutic target.Since ISO disrupted mitochondrial metabolism, we hypothesized that it could synergize with cuproptosis to amplify tumor killing. Initially, MTT assays revealed that ES-Cu could significantly inhibit the growth of gastric cancer cells, exhibiting little effect on normal gastric epithelial cells (Fig. 3A). This indicated that ES-Cu could selectively target and eliminate gastric cancer cells. To confirm that this phenomenon involved cuproptosis, the copper chelator TTM (10μmol/L) was added, resulting in significant restoration of cell viability (Fig. 3B). Subsequently, an increase in oligomerized DLAT levels was observed following ES-Cu treatment using immunofluorescence assays (Fig. 3E). Western blot analysis further revealed that the combination of ES-Cu led to an increase in DLAT expression in insoluble proteins (Fig. 3I), indicating that the ES-Cu combination promotes DLAT oligomerization. Western blot analysis showed that ES-Cu treatment reduced the expression levels of iron-sulfur cluster proteins ACO2/ETFDH/LIAS. Thus, we demonstrated that ES-Cu induces cuproptosis in gastric cancer cells. We hypothesized whether ISO could enhance the cytotoxic effect when combined with the established cuproposis model (ES-Cu). The effects of this combination were assessed on the viability, proliferation, and migration of gastric cancer cells AGS and HGC27. The MTT assay showed that the combination of ISO (3μmol/L, 6μmol/L, 9μmol/L) and ES (1.25nm, 2.5nm, 5nm, 10nm, 20nm)-Cu (10μmol/L) inhibited cancer cell viability in all cell lines (Fig. 3A), while the use of copper chelator TTM (10μmol/L) effectively reduced cell toxicity (Fig. 3B). Cell cloning experiments further confirmed the inhibitory effect of the combination group on cell proliferation. Compared to other groups, the colony formation of the ISO (6μmol/L) and ES (1.25μmol/L) - Cu (10μmol/L) combination group was significantly reduced (Fig. 3D). The cell scratch assay was used to evaluate the inhibitory effects of ISO and ES-Cu on the migration of AGS and HGC27 cells. We found that, compared to the control group, the combination group exhibited the smallest area of cell migration after 48 hours (Fig. 3C). These results suggest that ISO can enhance the cuproptosis effect in gastric cancer cells. In addition, JC-1 staining was used to evaluate the changes in mitochondrial function in cells, revealing that the combination group experienced the most severe mitochondrial damage, with the strongest green fluorescence and the weakest red fluorescence intensity (Fig. 3F). Finally, DCF/DHE staining showed the highest fluorescence intensity in the combination group, indicating an increase in intracellular oxidative stress levels (Fig. 3G). These experimental data further indicate that the

combination of ISO and ES-Cu leads to severe mitochondrial dysfunction. Immunofluorescence assay showed that the oligomerization level of DLAT was further increased in the combination group compared to other groups (Fig. 3E). Western blot analysis revealed that ISO significantly enhanced ES-Cu-induced DLAT oligomerization (Fig. 3E, I) and suppressed iron-sulfur cluster proteins (ACO2/ETFDH/LIAS, Fig. 3H), confirming synergistic activation of cuproptosis. Therefore, these results confirmed that ISO could induce the death of gastric cancer cells via a synergistic cuproptosis mechanism.

3.4. FDX1 is the critical mediator of ISO/ES-Cu synergistic cuproptosis

Since FDX1, a key regulator of copper ion reduction and DLAT lipoylation, is central to cuproptosis induction, we next assessed whether ISO/ES-Cu synergy operates through this target.We first assessed FDX1 expression level (Fig. 4A). Molecular docking and dynamics confirmed direct binding of ISO and ES-Cu to FDX1 (Fig. 4B-C), while FDX1 knockdown abrogated the synergistic cell death (Fig. 5D-E) and DLAT aggregation (Fig. 4F).To assess this, molecular docking simulations were performed, revealing the presence of visible hydrogen bonds between FDX1 and the components of the ISO-cuproptosis combination, with binding energies of -5.3 kcal mol-1 and − 7.0 kcal mol-1, respectively (Fig. 4B). This indicated direct and favorable interactions between FDX1 and the combined agents. Subsequently, MD simulations were conducted, confirming stable interactions between FDX1 and the ISO-cuproptosis combination. These simulations showed that the binding of ISO and cuproptosis induced a more compact conformation of FDX1 molecules, reduced their surface area, and promoted the formation of many hydrogen bonds with the small molecules. The RMSD for the protein ultimately stabilized at around 1nm, and the Rg indicated a gradual contraction of the simulated protein, stabilizing at approximately 1.4 nm. Molecular dynamics simulations showed strong affinity and interaction between ISO and cuproptosis and FDX1 (Fig. 4C). To further validate the above results, an FDX1-deficient cellular model was generated using an FDX1-targeted siRNA transfection system in AGS/HGC27 cells. An MTT assay was used to evaluate the effect of ISO combined with copper death treatment on FDX1-deficient gastric cancer cells after 48 hours. The results showed that the viability of FDX1-deficient cells in the combined group was significantly higher than that of the vehicle group, indicating that knocking out FDX1 reduced the sensitivity of gastric cancer cells to ISO and ES-Cu, thereby weakening the cuproptosis effect (Fig. 4E). The plate cloning experiment also confirmed this result, showing that the FDX1 deficient cell colony forming ability of the combined group was higher than that of the vehicle group (Fig. 4D). Subsequently, immunofluorescence assay revealed that the oligomerization intensity of DLAT in the combined group was significantly higher than that in the vehicle group (Fig. 4F), indicating that knocking down FDX1 could effectively reverse the cuproptosis effect. The above findings preliminarily indicate that FDX1 may serve as a therapeutic target for enhancing the synergistic inhibition of gastric cancer cell growth by ISO and cuproptosis.

3.5. Combined application of ISO and cisplatin (CIS) to kill gastric cancer cells

It is well-established that the chemotherapy drug CIS exhibits limited efficacy due to drug resistance. We next evaluated ISO's clinical translatability by combining it with cisplatin, a frontline gastric cancer drug.We evaluated the effects of the combination group on cell viability, proliferation, migration, and death markers in AGS and HGC27. MTT assays showed that the combination of ISO (3μmol/L) and CIS (2μmol/L) exhibited the most effective inhibition of cancer cell viability in both cell lines (Fig. 5A). Cell cloning assay further confirmed the inhibitory effect on cell proliferation, and compared with the control group, the ISO-CIS group showed a significant reduction in colony formation (Fig. 5C). Meanwhile, the cell scratch assay demonstrated that the ISO-CIS group exhibited the smallest migration area, indicating a strong inhibitory effect on cell migration (Fig. 5B). In addition, DCF/DHE staining showed the highest fluorescence intensity in these combination groups, indicating an increase in intracellular oxidative stress levels (Fig. 5D). Finally, JC-1 staining revealed that mitochondrial damage was most severe in cells treated with ISO-CIS, characterized by the strongest green fluorescence and weakest red fluorescence intensity (Fig. 5E). Western blot analysis showed that the combination of ISO and CIS significantly inhibited the expression of cycle-related proteins CyclinD1/CDK2 and enhanced the expression of P21/P27 proteins in AGS and HGC27, hindering cell cycle progression (Fig. 5F). In the meantime, the combination of ISO and CIS significantly downregulated the expression of apoptotic proteins Bax, Bad, and cleaved caspase-9/caspase-9 in the mitochondrial pathway, upregulated the expression of anti-apoptotic protein Bcl-2, which may contribute to the observed growth inhibition of gastric cancer cells (Fig. 5G). Based on the above experimental data analysis, we preliminarily demonstrated that the combination of ISO and CIS exhibits a significant inhibitory effect on the growth of gastric cancer cells.

4. Discussion

Gastric cancer ranks as the fifth most common cancer worldwide, with an estimated 1.29 million new cases reported in 2022. Notably, nearly half (43%) of these cases are concentrated in China[23]. The insidious nature of early symptoms and a high rate of chemotherapy resistance contribute to the diagnosis of most gastric cancer patients at locally advanced or metastatic stages (III-IV). This translates to a dismal 5-year survival rate of only 20–30%, thereby classifying gastric cancer among digestive tract tumors with the poorest prognoses[24]. While the implementation of targeted therapy and immunotherapy has enhanced the prognosis for certain patients, the overall outlook for gastric cancer remains unfavorable. This is primarily attributed to its significant heterogeneity, pronounced invasiveness, and complex biological characteristics. Furthermore, existing treatment modalities have yet to overcome limitations concerning drug resistance and the sustained efficacy of treatments. [25–26]. Consequently, this persistent clinical challenge urgently necessitates the identification of novel intervention strategies from natural sources, which offer multi-target mechanisms to overcome drug resistance and enhance therapeutic efficacy.

Natural products are highly valued for their structural diversity, biological activity, and low toxicity[27]. They play a crucial role in disease treatment, especially in overcoming tumor cell resistance, which may

contribute to effective tumor therapy[28]. Among these natural compounds, bisbenzylisoquinoline alkaloids—particularly isoliensinine (ISO) derived from lotus seed hearts—have emerged as promising candidates due to their documented anti-tumor properties across multiple cancer types, including liver and breast cancer. Its role is closely related to regulating Bcl-2 family proteins, activating the caspase pathway, and inducing the accumulation of ROS[21]. In this study, we provided hitherto undocumented evidence that ISO can significantly inhibit the proliferation, migration, and colony formation abilities of gastric cancer cells (AGS, HGC27, MFC) *in vitro* without damaging normal gastric epithelial cells. Regarding traditional molecular targets, we initially validated the regulatory effect of ISO on cyclin. Western blot analysis revealed that ISO significantly downregulated the expression of Cyclin D1, inhibited G1/S phase transition, and led to cell cycle arrest in G1 phase. Besides, ISO upregulated the expression of CDK inhibitory proteins p21 and p27 by activating p53-dependent or non-dependent pathways, thereby inhibiting CDK activity, further blocking cell cycle progression, and ultimately inhibiting gastric cancer cell proliferation. Next, we focused on apoptosis, the most common and extensively studied form of programmed cell death. Our findings found that ISO induced the release of pro-apoptotic factors, which could bind to Apaf-1 in the cytoplasm to form apoptotic complexes, thereby activating Caspase-9 and ultimately leading to cell apoptosis. Meanwhile, ISO downregulated anti-apoptotic proteins (such as Bcl-2) and upregulated pro-apoptotic proteins (such as Bax and Bad), thereby influencing the induction of cell apoptosis. It can thus be inferred that ISO can promote apoptosis of gastric cancer cells. *In vivo* studies further demonstrated that ISO significantly delayed the tumor growth of MFC cells in BALB/c nude mice, which was also confirmed by Ki67 immunohistochemistry results. Meanwhile, HE staining of major tissues and organs in mice confirmed the safety profile of ISO. In summary, our investigations into traditional targets have preliminarily demonstrated that ISO exerts an inhibitory effect on the growth of gastric cancer cells. Moreover, ISO-induced apoptosis was characterized as mitochondrial-dependent, evidenced by the release of pro-apoptotic factors and the observed mitochondrial dysfunction. This disruption of mitochondrial homeostasis raised the intriguing possibility that ISO might synergize with other therapeutic modalities targeting mitochondrial vulnerabilities.

Next, we sought to explore the mechanism by which ISO inhibits the growth of gastric cancer cells. RNA sequencing revealed that ISO's inhibitory effect on gastric cancer cell growth was linked to DNA replication, the cell cycle, the MAPK pathway, and the PI3K-AKT pathway. The prominent enrichment of the MAPK pathway—a critical regulator of cellular stress responses and mitochondrial function[29] [30] [31] [32] — led us to hypothesize that MAPK activation may functionally link ISO-induced oxidative stress to mitochondrial dysfunction. To test this hypothesis, we first examined the activation status of the MAPK pathway. Western blot analysis confirmed that ISO treatment significantly and concentration-dependently upregulated the phosphorylation (activation) of both JNK and p38 proteins in gastric cancer cells. Given the established role of JNK/p38 MAPK activation in mitochondrial perturbation—including loss of membrane potential and ROS generation—and our validation of ISO-induced MAPK activation, we next examined functional consequences on mitochondrial integrity. JC-1 staining revealed a pronounced, concentration-dependent loss of mitochondrial membrane potential following ISO treatment, indicative of severe mitochondrial dysfunction. Concurrently, DCFH-DA and DHE staining demonstrated a

significant, dose-dependent increase in intracellular reactive oxygen species (ROS) levelst. Collectively, these data establish that ISO induces profound mitochondrial damage and oxidative stress in gastric cancer cells. Critically, the concomitant activation of the stress-responsive JNK/p38 MAPK signaling axis provides a mechanistic basis for ISO-induced mitochondrial dysfunction, ultimately driving cell cycle arrest and apoptosis.

This disruption of mitochondrial homeostasis raised the intriguing possibility that ISO might synergize with cuproptosis inducers.Cuproptosis is a newly discovered form of programmed cell death, first proposed in 2022, which reveals the unique pathway through which copper ions disrupt mitochondrial metabolism and trigger cell death[33]. Its core feature is directly triggered by excessive copper ions (especially abnormal accumulation of copper in mitochondria), which is significantly different from traditional mechanisms such as apoptosis, necrosis, or ferroptosis[34]. The occurrence of copper death depends on the increase in intracellular concentration of free copper ions, especially the excessive accumulation of copper in mitochondria. When copper ions bind to lipid-modified mitochondrial enzymes in the tricarboxylic acid cycle (TCA cycle), such as the pyruvate dehydrogenase complex, it leads to the aggregation of DLAT and the loss of iron sulfur cluster (Fe-S) proteins, thereby disrupting mitochondrial function. This protein toxicity further triggers mitochondrial respiratory chain dysfunction, leading to a breakdown of energy metabolism and an increase in ROS, ultimately driving cells towards death[35–36]. Research has shown that Elesclomol is an oxidative stress inducer that binds to copper ions (Cu^{2+}) to form a complex, targeting delivery to mitochondria and thereby triggering cuproptosis[37]. Copper ion chelating agents (such as TTM) can reduce their toxic effects by binding to free copper ions, thereby reversing the occurrence of cuproptosis[38].

FDX1 is a mitochondrial iron-sulfur cluster protein that plays a critical role in cellular copper ion homeostasis and energy metabolism[39–40]. Research has shown that FDX1 is the core regulatory factor of cuproptosis, which can initiate the conversion of extracellular divalent Cu^{2+} into more toxic intracellular cuprous ions (Cu^{+}). Its absence leads to loss of protein acylation, thereby preventing cell cuproptosis[41]. Notably, TCGA analysis revealed that the mRNA level of the key regulatory factor FDX1 for cuproptosis in kidney cancer tissue was significantly upregulated compared to normal tissue and was associated with a shortened overall survival[42–44]. This suggests that FDX1 may be a potential target for cuproptosis intervention in gastric cancer. In addition, FDX1 promotes the abnormal aggregation of acylated proteins and the reduction of iron-sulfur cluster proteins, leading to protein toxicity stress and ultimately causing cell death[45–46].

Given the central role of mitochondrial integrity in cellular survival and the emergence of cuproptosis as a novel mitochondrial-targeted cell death pathway triggered by copper overload and protein aggregation, we hypothesized that exacerbating mitochondrial dysfunction through the combined application of ISO and cuproptosis inducers could offer a potent and synergistic therapeutic strategy against GC. In this study, the combination of ISO and cuproptosis synergistically induced gastric cancer cell death, with the core mechanism involving FDX1-mediated mitochondrial dysfunction and copper homeostasis

disruption. The ES-Cu model successfully mimics cuproptosis characteristics, presenting enhanced DLAT oligomerization and decreased expression of iron-sulfur cluster proteins (ACO2, ETFDH, LIAS), with its cytotoxicity reversible by a copper chelator (TTM), consistent with the copper ion overload dependency of cuproptosis. Combined treatment with ISO further exacerbated these effects: the synergistic action of increased DLAT oligomerization and inhibition of iron-sulfur cluster protein expression directly disrupted mitochondrial respiratory chain function (confirmed by JC-1 and DCF/DHE staining), leading to irreversible proteinotoxic stress. Notably, FDX1 has been identified as a key target in the combined therapy. Western blot results showed significant upregulation of FDX1 in the combined treatment group, while molecular docking and molecular dynamics experiments further indicated that ISO and ES-Cu could directly bind to FDX1, suggesting that both can enhance FDX1 activity by stabilizing its conformation. The abrogation of the synergistic effect after FDX1 knockout confirmed its central role in the combined application.

While ISO/FDX1-mediated cuproptosis synergy offers a novel mechanism, clinical translation requires evaluation of ISO with standard chemotherapy to address broader patient populations. Beyond its direct antitumor effects and synergistic potential with novel cuproptosis inducers, we further evaluated the clinical translatability of ISO by examining its combination with cisplatin (CIS), a cornerstone chemotherapeutic agent in gastric cancer treatment. Consistent with the rationale for combining natural products with chemotherapy to overcome resistance and reduce toxicity[47–48]. Research has shown that curcumin enhances the effects of cisplatin and 5-fluorouracil on colorectal and ovarian cancer by inhibiting the NF-κB pathway and downregulating Bcl-2[49]. Resveratrol in grapes and berries can induce autophagy by activating SIRT1 and improve the efficacy of gemcitabine in pancreatic cancer.[50] Furthermore, artemisinin derivatives (such as dihydroartemisinin) enhance the anticancer effect of cisplatin in cisplatin-resistant ovarian cancer cells through mTOR inhibition[51]. Sulforaphane potentiates the efficacy of chemoradiotherapy in glioblastoma by selectively targeting thioredoxin reductase[52], while toosendanin sensitizes cancer cells to chemotherapy by blocking protective autophagy[53]. In the present study, the combination of ISO and the chemotherapy drug cisplatin was found to enhance anti-tumor efficacy. This combined application significantly reduced the proliferation, migration, colony formation ability, and mitochondrial function of gastric cancer AGS and HGC27 cells. In addition, the combination therapy with ISO and CIS resulted in an increase in oxidative stress levels in cancer cells. Notably, in terms of clinical translation, the inherent complexity difference between *in vitro* experiments and *in vivo* tumor microenvironment leads to inconsistent efficacy. Currently, most studies remain in the preclinical stage, and advancing to phase II/III clinical trials is essential to verify safety and effectiveness.

This study delineates the anti-gastric cancer mechanisms of ISO, demonstrating its induction of mitochondrial apoptosis and G1/S cell cycle arrest. Critically, we establish an innovative combinatorial strategy wherein ISO synergizes with the cuproptosis inducer ES-Cu through specific targeting of FDX1. Mechanistically, ISO-ES-Cu co-targeting of FDX1 triggers irreversible mitochondrial dysfunction,

characterized by exacerbated DLAT oligomerization and ROS overproduction. This novel regulatory mechanism offers a promising therapeutic strategy for gastric cancer.

5. Conclusion

In summary,This study delineates ISO as a mitochondrial-targeting agent that suppresses gastric cancer through intrinsic apoptosis and G1/S arrest. Crucially, we establish that ISO cooperatively targets FDX1 with cuproptosis inducers (ES-Cu), amplifying DLAT oligomerization and ROS accumulation to potentiate copper-dependent cell death. This FDX1-directed synergy defines a novel combinatorial strategy wherein ISO converts mitochondrial vulnerability into enhanced cuproptotic lethality. Collectively, these findings unveil ISO as a dual-functional agent that not only exerts intrinsic anti-tumor activity but also pioneers a precision approach for overcoming chemotherapy resistance in gastric cancer.

Abbreviations

CIS
cisplatin
DCF
2 ',7' - dichlorodihydrofluorescein diacetate
DHE
Dihydroethidium
ES
Elesclomol
GEO
Gene Expression Omnibus
H&E
hematoxylin and eosin
ISO
Isoliensinine
KEGG
Kyoto encyclopedia of genes and genomes
MTT
3-(4,5-dimethylthiazol-2-yl)-2,5-diphenyltetrazolium bromide
PI
Propidium Iodide
PVDF
polyvinylidene fluoride
p-JNK
phosphorylated JNK
p-P38
phosphorylated P38

ROS
reactive oxygen species
siRNA
Small interfering RNA
TCGA
the Cancer Genome Atlas.

Declarations

Ethics approval and consent to participate

No ethical approval is required for this study.

Consent for publication

Not applicable.

Acknowledgements

We gratitude the experimental support on the public platform of Qingdao University Biomedical Center. We gratitude the experimental support on the medical research center public platform of The Affiliated Hospital of Qingdao University. We thank Home for Researchers editorial team (www.home-for-researchers.com) for language editing service.

Authors' contributions

The research was planned by SYZ, carried out by SYZ and YYF, with technical assistance from KC, JLS and YYL. SYZ, YYF, SSW, WWQ and WSQ then analysed the data and prepared the report.

Funding

This study was supported by Beijing Xisike Clinical Oncology Research Foundation（Y2019-AZZD-0471）.

Competing interests

The authors declare no potential conflicts of interest.

Clinical trial number

not applicable.

Data Availability

The article and supplementary materials contain the data for this investigation. The corresponding author can give raw data or particular details of the experimental operation as long as the request is

legitimate.

References

1. López, M.J., J. Carbajal, A.L. Alfaro, L.G. Saravia, D. Zanabria, J.M. Araujo, L. Quispe, A. Zevallos, J.L. Buleje, C.E. Cho, M. Sarmiento, J.A. Pinto, and W. Fajardo, Characteristics of gastric cancer around the world. Crit Rev Oncol Hematol, 2023 10.1016/j.critrevonc.2022.103841
2. Thrift, A.P. and H.B. El-Serag, Burden of Gastric Cancer. Clin Gastroenterol Hepatol, 2020 10.1016/j.cgh.2019.07.045 PMC8859863
3. Bray, F., M. Laversanne, H. Sung, J. Ferlay, R.L. Siegel, I. Soerjomataram, and A. Jemal, Global cancer statistics 2022: GLOBOCAN estimates of incidence and mortality worldwide for 36 cancers in 185 countries. CA Cancer J Clin, 2024 10.3322/caac.21834
4. Hato, S.V., A. Khong, I.J. de Vries, and W.J. Lesterhuis, Molecular pathways: the immunogenic effects of platinum-based chemotherapeutics. Clin Cancer Res, 2014 10.1158/1078-0432.Ccr-13-3141
5. Ilic, M. and I. Ilic, Epidemiology of stomach cancer. World J Gastroenterol, 2022 10.3748/wjg.v28.i12.1187 PMC8968487
6. Wakatsuki, T., N. Yamamoto, T. Sano, K. Chin, H. Kawachi, D. Takahari, M. Ogura, T. Ichimura, I. Nakayama, H. Osumi, T. Matsushima, M. Suenaga, E. Shinozaki, N. Hiki, Y. Ishikawa, and K. Yamaguchi, Clinical impact of intratumoral HER2 heterogeneity on trastuzumab efficacy in patients with HER2-positive gastric cancer. J Gastroenterol, 2018 10.1007/s00535-018-1464-0 PMC6209002
7. Zhao, T.T., H. Xu, H.M. Xu, Z.N. Wang, Y.Y. Xu, Y.X. Song, S.C. Yin, X.Y. Liu, and Z.F. Miao, The efficacy and safety of targeted therapy with or without chemotherapy in advanced gastric cancer treatment: a network meta-analysis of well-designed randomized controlled trials. Gastric Cancer, 2018 10.1007/s10120-018-0813-2
8. Haque, E., A. Esmail, I. Muhsen, H. Salah, and M. Abdelrahim, Recent Trends and Advancements in the Diagnosis and Management of Gastric Cancer. Cancers (Basel), 2022 10.3390/cancers14225615 PMC9688354
9. Luo, D., Y. Liu, Z. Lu, and L. Huang, Targeted therapy and immunotherapy for gastric cancer: rational strategies, novel advancements, challenges, and future perspectives. Mol Med, 2025 10.1186/s10020-025-01075-y PMC11806620
10. Lu, Y.Y., C.Y. Zhu, Y.X. Ding, B. Wang, S.F. Zhao, J. Lv, S.M. Chen, S.S. Wang, Y. Wang, R. Wang, W.S. Qiu, and W.W. Qi, Cepharanthine, a regulator of keap1-Nrf2, inhibits gastric cancer growth through oxidative stress and energy metabolism pathway. Cell Death Discov, 2023 10.1038/s41420-023-01752-z PMC10716385
11. Atanasov, A.G., S.B. Zotchev, V.M. Dirsch, and C.T. Supuran, Natural products in drug discovery: advances and opportunities. Nat Rev Drug Discov, 2021 10.1038/s41573-020-00114-z PMC7841765

12. Sharifi-Rad, J., C. Quispe, J.K. Patra, Y.D. Singh, M.K. Panda, G. Das, C.O. Adetunji, O.S. Michael, O. Sytar, L. Polito, J. Živković, N. Cruz-Martins, M. Klimek-Szczykutowicz, H. Ekiert, M.I. Choudhary, S.A. Ayatollahi, B. Tynybekov, F. Kobarfard, A.C. Muntean, I. Grozea, S.D. Daştan, M. Butnariu, A. Szopa, and D. Calina, Paclitaxel: Application in Modern Oncology and Nanomedicine-Based Cancer Therapy. Oxid Med Cell Longev, 2021 10.1155/2021/3687700 PMC8545549
13. Dasari, S., S. Njiki, A. Mbemi, C.G. Yedjou, and P.B. Tchounwou, Pharmacological Effects of Cisplatin Combination with Natural Products in Cancer Chemotherapy. Int J Mol Sci, 2022 10.3390/ijms23031532 PMC8835907
14. Lu, Y.Y., Y.Y. Fang, S.S. Wang, J. Guo, J.L. Song, L. Zhu, Z.K. Lin, R. Wang, S.Y. Zhang, W.S. Qiu, and W.W. Qi, Cepharanthine sensitizes gastric cancer cells to chemotherapy by targeting TRIB3-FOXO3-FOXM1 axis to inhibit autophagy. Phytomedicine, 2024 10.1016/j.phymed.2024.156161
15. Wang, W., X. Yuan, J. Mu, Y. Zou, L. Xu, J. Chen, X. Zhu, B. Li, Z. Zeng, X. Wu, Z. Yin, and Q. Wang, Quercetin induces MGMT(+) glioblastoma cells apoptosis via dual inhibition of Wnt3a/β-Catenin and Akt/NF-κB signaling pathways. Phytomedicine, 2023 10.1016/j.phymed.2023.154933
16. Li, D., Y. Li, L. Chen, C. Gao, B. Dai, W. Yu, H. Yang, J. Pi, and X. Bian, Natural Product Auraptene Targets SLC7A11 for Degradation and Induces Hepatocellular Carcinoma Ferroptosis. Antioxidants (Basel), 2024 10.3390/antiox13081015 PMC11351406
17. Feng, L., T.Z. Wu, X.R. Guo, Y.J. Wang, X.J. Wang, S.X. Liu, R. Zhang, Y. Ma, N.H. Tan, J.L. Bian, and Z. Wang, Discovery of Natural Resorcylic Acid Lactones as Novel Potent Copper Ionophores Covalently Targeting PRDX1 to Induce Cuproptosis for Triple-Negative Breast Cancer Therapy. ACS Cent Sci, 2025 10.1021/acscentsci.4c02188 PMC11869127
18. Cheng, Y., H.L. Li, Z.W. Zhou, H.Z. Long, H.Y. Luo, D.D. Wen, L. Cheng, and L.C. Gao, Isoliensinine: A Natural Compound with "Drug-Like" Potential. Front Pharmacol, 2021 10.3389/fphar.2021.630385 PMC8100667
19. Manogaran, P., A. Anandan, and V. Vijaya Padma, Isoliensinine augments the therapeutic potential of paclitaxel in multidrug-resistant colon cancer stem cells and induced mitochondria-mediated cell death. J Biochem Mol Toxicol, 2023 10.1002/jbt.23395
20. Zhang, X., X. Wang, T. Wu, B. Li, T. Liu, R. Wang, Q. Liu, Z. Liu, Y. Gong, and C. Shao, Isoliensinine induces apoptosis in triple-negative human breast cancer cells through ROS generation and p38 MAPK/JNK activation. Sci Rep, 2015 10.1038/srep12579 PMC4518223
21. Li, H.L., Y. Cheng, Z.W. Zhou, H.Z. Long, H.Y. Luo, D.D. Wen, L. Cheng, and L.C. Gao, Isoliensinine induces cervical cancer cell cycle arrest and apoptosis by inhibiting the AKT/GSK3α pathway. Oncol Lett, 2022 10.3892/ol.2021.13126 PMC8607237
22. Shu, G., L. Yue, W. Zhao, C. Xu, J. Yang, S. Wang, and X. Yang, Isoliensinine, a Bioactive Alkaloid Derived from Embryos of Nelumbo nucifera, Induces Hepatocellular Carcinoma Cell Apoptosis through Suppression of NF-κB Signaling. J Agric Food Chem, 2015 10.1021/acs.jafc.5b02993
23. Yang, W.J., H.P. Zhao, Y. Yu, J.H. Wang, L. Guo, J.Y. Liu, J. Pu, and J. Lv, Updates on global epidemiology, risk and prognostic factors of gastric cancer. World J Gastroenterol, 2023

10.3748/wjg.v29.i16.2452 PMC10167900

24. Smyth, E.C., M. Nilsson, H.I. Grabsch, N.C. van Grieken, and F. Lordick, Gastric cancer. Lancet, 2020 10.1016/s0140-6736(20)31288-5
25. Guan, W.L., Y. He, and R.H. Xu, Gastric cancer treatment: recent progress and future perspectives. J Hematol Oncol, 2023 10.1186/s13045-023-01451-3 PMC10225110
26. Ma, Q., H. Jiang, L. Ma, G. Zhao, Q. Xu, D. Guo, N. He, H. Liu, Z. Meng, J. Liu, L. Zhu, Q. Lin, X. Wu, M. Li, S. Luo, J. Fang, and Z. Lu, The moonlighting function of glycolytic enzyme enolase-1 promotes choline phospholipid metabolism and tumor cell proliferation. Proc Natl Acad Sci U S A, 2023 10.1073/pnas.2209435120 PMC10104498
27. Chen, T., Z. Xiao, X. Liu, T. Wang, Y. Wang, F. Ye, J. Su, X. Yao, L. Xiong, and D.H. Yang, Natural products for combating multidrug resistance in cancer. Pharmacol Res, 2024 10.1016/j.phrs.2024.107099
28. Naeem, A., P. Hu, M. Yang, J. Zhang, Y. Liu, W. Zhu, and Q. Zheng, Natural Products as Anticancer Agents: Current Status and Future Perspectives. Molecules, 2022 10.3390/molecules27238367 PMC9737905
29. Wang, H.B. and X.Q. Ma, Activation of JNK/p38 pathway is responsible for α-methyl-n-butylshikonin induced mitochondria-dependent apoptosis in SW620 human colorectal cancer cells. Asian Pac J Cancer Prev, 2014 10.7314/apjcp.2014.15.15.6321
30. Zhu, Y., Y. Jiang, L. Shi, L. Du, X. Xu, E. Wang, Y. Sun, X. Guo, B. Zou, H. Wang, C. Wang, L. Sun, and Y. Zhen, 7-O-Geranylquercetin induces apoptosis in gastric cancer cells via ROS-MAPK mediated mitochondrial signaling pathway activation. Biomed Pharmacother, 2017 10.1016/j.biopha.2016.12.095
31. Yu, X., J. Zhong, L. Yan, J. Li, H. Wang, Y. Wen, and Y. Zhao, Curcumin exerts antitumor effects in retinoblastoma cells by regulating the JNK and p38 MAPK pathways. Int J Mol Med, 2016 10.3892/ijmm.2016.2676
32. Serra, G., M. Deiana, J.P.E. Spencer, and G. Corona, Olive Oil Phenolics Prevent Oxysterol-Induced Proinflammatory Cytokine Secretion and Reactive Oxygen Species Production in Human Peripheral Blood Mononuclear Cells, Through Modulation of p38 and JNK Pathways. Mol Nutr Food Res, 2017 10.1002/mnfr.201700283 PMC5765427
33. Kahlson, M.A. and S.J. Dixon, Copper-induced cell death. Science, 2022 10.1126/science.abo3959
34. Tang, D., X. Chen, and G. Kroemer, Cuproptosis: a copper-triggered modality of mitochondrial cell death. Cell Res, 2022 10.1038/s41422-022-00653-7 PMC9061796
35. Chen, L., J. Min, and F. Wang, Copper homeostasis and cuproptosis in health and disease. Signal Transduct Target Ther, 2022 10.1038/s41392-022-01229-y PMC9681860
36. Li, S.R., L.L. Bu, and L. Cai, Cuproptosis: lipoylated TCA cycle proteins-mediated novel cell death pathway. Signal Transduct Target Ther, 2022 10.1038/s41392-022-01014-x PMC9106713
37. Tarin, M., M. Babaie, H. Eshghi, M.M. Matin, and A.S. Saljooghi, Elesclomol, a copper-transporting therapeutic agent targeting mitochondria: from discovery to its novel applications. J Transl Med,

2023 10.1186/s12967-023-04533-5 PMC10589935

38. Xie, J., Y. Yang, Y. Gao, and J. He, Cuproptosis: mechanisms and links with cancers. Mol Cancer, 2023 10.1186/s12943-023-01732-y PMC9990368
39. Yang, L., Y. Zhang, Y. Wang, P. Jiang, F. Liu, and N. Feng, Ferredoxin 1 is a cuproptosis-key gene responsible for tumor immunity and drug sensitivity: A pan-cancer analysis. Front Pharmacol, 2022 10.3389/fphar.2022.938134 PMC9532935
40. Zulkifli, M., A.N. Spelbring, Y. Zhang, S. Soma, S. Chen, L. Li, T. Le, V. Shanbhag, M.J. Petris, T.Y. Chen, M. Ralle, D.P. Barondeau, and V.M. Gohil, FDX1-dependent and independent mechanisms of elesclomol-mediated intracellular copper delivery. Proc Natl Acad Sci U S A, 2023 10.1073/pnas.2216722120 PMC10013847
41. Wang, Z., D. Jin, S. Zhou, N. Dong, Y. Ji, P. An, J. Wang, Y. Luo, and J. Luo, Regulatory roles of copper metabolism and cuproptosis in human cancers. Front Oncol, 2023 10.3389/fonc.2023.1123420 PMC10076572
42. Schulz, V., S. Basu, S.A. Freibert, H. Webert, L. Boss, U. Mühlenhoff, F. Pierrel, L.O. Essen, D.M. Warui, S.J. Booker, O. Stehling, and R. Lill, Functional spectrum and specificity of mitochondrial ferredoxins FDX1 and FDX2. Nat Chem Biol, 2023 10.1038/s41589-022-01159-4 PMC10873809
43. Yao, Y., H. Chen, M. Lou, and T. Chen, Cuproptosis-related gene FDX1 as a prognostic biomarker for kidney renal clear cell carcinoma correlates with immune checkpoints and immune cell infiltration. Front Genet, 2023 10.3389/fgene.2023.1071694 PMC9900009
44. Zhang, W.T., Y.M. Gong, C.Y. Zhang, J.S. Pan, T. Huang, and Y.X. Li, A Novel Cuprotosis-Related Gene FDX1 Signature for Overall Survival Prediction in Clear Cell Renal Cell Carcinoma Patients. Biomed Res Int, 2022 10.1155/2022/9196540 PMC9467705
45. Abdullah, K.M., J.B. Kaushal, S. Takkar, G. Sharma, Z.W. Alsafwani, R. Pothuraju, S.K. Batra, and J.A. Siddiqui, Copper metabolism and cuproptosis in human malignancies: Unraveling the complex interplay for therapeutic insights. Heliyon, 2024 10.1016/j.heliyon.2024.e27496 PMC10938126
46. Dreishpoon, M.B., N.R. Bick, B. Petrova, D.M. Warui, A. Cameron, S.J. Booker, N. Kanarek, T.R. Golub, and P. Tsvetkov, FDX1 regulates cellular protein lipoylation through direct binding to LIAS. J Biol Chem, 2023 10.1016/j.jbc.2023.105046 PMC10462841
47. Castañeda, A.M., C.M. Meléndez, D. Uribe, and J. Pedroza-Díaz, Synergistic effects of natural compounds and conventional chemotherapeutic agents: recent insights for the development of cancer treatment strategies. Heliyon, 2022 10.1016/j.heliyon.2022.e09519 PMC9163513
48. Zhou, L., L. Qi, L. Jiang, P. Zhou, J. Ma, X. Xu, and P. Li, Antitumor activity of gemcitabine can be potentiated in pancreatic cancer through modulation of TLR4/NF-κB signaling by 6-shogaol. Aaps j, 2014 10.1208/s12248-013-9558-3 PMC3933586
49. Shakibaei, M., P. Kraehe, B. Popper, P. Shayan, A. Goel, and C. Buhrmann, Curcumin potentiates antitumor activity of 5-fluorouracil in a 3D alginate tumor microenvironment of colorectal cancer. BMC Cancer, 2015 10.1186/s12885-015-1291-0 PMC4406109

50. Buhrmann, C., M. Yazdi, B. Popper, P. Shayan, A. Goel, B.B. Aggarwal, and M. Shakibaei, Resveratrol Chemosensitizes TNF-β-Induced Survival of 5-FU-Treated Colorectal Cancer Cells. Nutrients, 2018 10.3390/nu10070888 PMC6073304
51. Feng, X., L. Li, H. Jiang, K. Jiang, Y. Jin, and J. Zheng, Dihydroartemisinin potentiates the anticancer effect of cisplatin via mTOR inhibition in cisplatin-resistant ovarian cancer cells: involvement of apoptosis and autophagy. Biochem Biophys Res Commun, 2014 10.1016/j.bbrc.2014.01.053
52. Ge, Y., Z. Ge, F. Tian, X. Tai, D. Chen, S. Sun, Z. Shi, J. Yin, G. Wei, D. Li, L. Wang, W. Xu, M. Tong, F. Liu, L. Zhao, X. Qian, and X. Ge, Sulforaphane potentiates the efficacy of chemoradiotherapy in glioblastoma by selectively targeting thioredoxin reductase 1. Cancer Lett, 2024 10.1016/j.canlet.2024.217429
53. Dong, Y., G. Zhu, S.F. Wang, K.A. Keon, J.L. Rubinstein, S.X. Zeng, S. Zhang, Q.L. Chen, J. Fu, M. Li, H.M. Shen, J.J. Lu, X.P. Chen, and J.H. Lu, Toosendanin, a novel potent vacuolar-type H(+)-translocating ATPase inhibitor, sensitizes cancer cells to chemotherapy by blocking protective autophagy. Int J Biol Sci, 2022 10.7150/ijbs.71041 PMC9066121

Figures

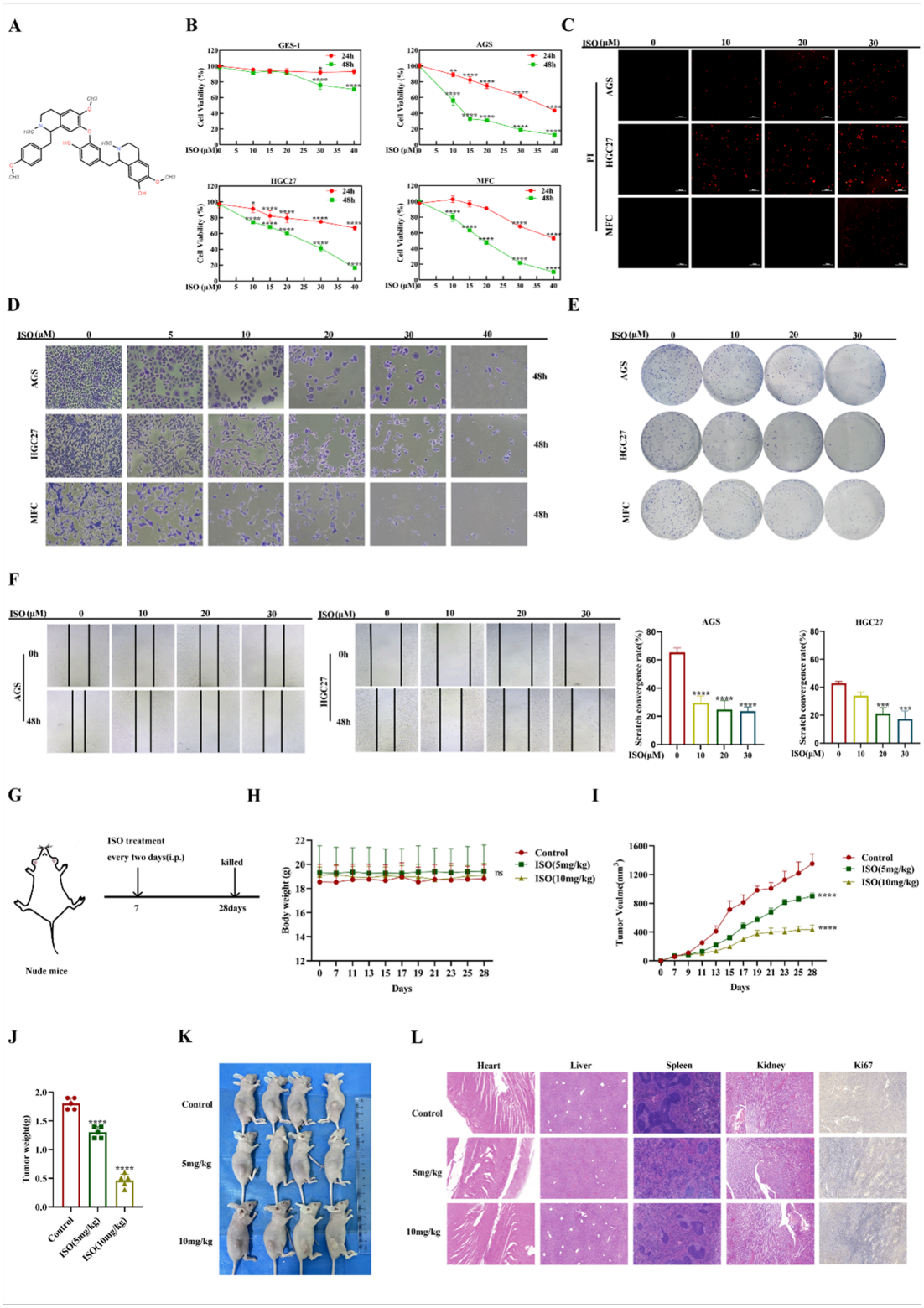


Figure 1

A. Chemical structure of ISO. **B.** Assessment of the viability of GES-1/AGS/HGC27/MFC cells treated with different concentrations of ISO for 24 or 48 hours using MTT assay (n=3). **C.** AGS/HGC27/MFC cells were exposed to ISO for 48 hours, and the degree of cell damage was evaluated by PI staining. Scale: 100μm. **D.** After ISO treatment of AGS/HGC27/MFC cells, cell morphology was observed by crystal violet staining.**E.** Cloning of AGS, HGC27, and MFC cells treated with ISO (0, 10, 20, and 30 μ mol/L) for 48

hours. **F.** Scratch test was used to determine the migration of AGS and HGC27 cells treated with ISO (0, 10, 20, and 30 μ mol/L) for 48 hours. Quantify scratch images by calculating the cell migration area (n=3) using Image J software. **G.** Animal experimental model diagram. **H-K.**Images of subcutaneous tumors in the BALB/c nude mouse model, as well as changes in tumor weight and volume and mouse body weight after drug treatment. **L.** Pathological changes of important organs such as heart, liver, spleen, and kidney in BALB/c nude mouse models treated with different drugs (H&E staining) and expression of Ki67 in tumor tissues of different groups (n=3) of MFC BALB/c nude mice (immunohistochemistry). Scale bar: 100 μ m. The data is expressed as mean ± standard deviation. Compared with the control group, the significance levels are as follows: * $p<0.05$, * * $p<0.01$, * * * $p<0.001$, * * * * $P<0.0001$

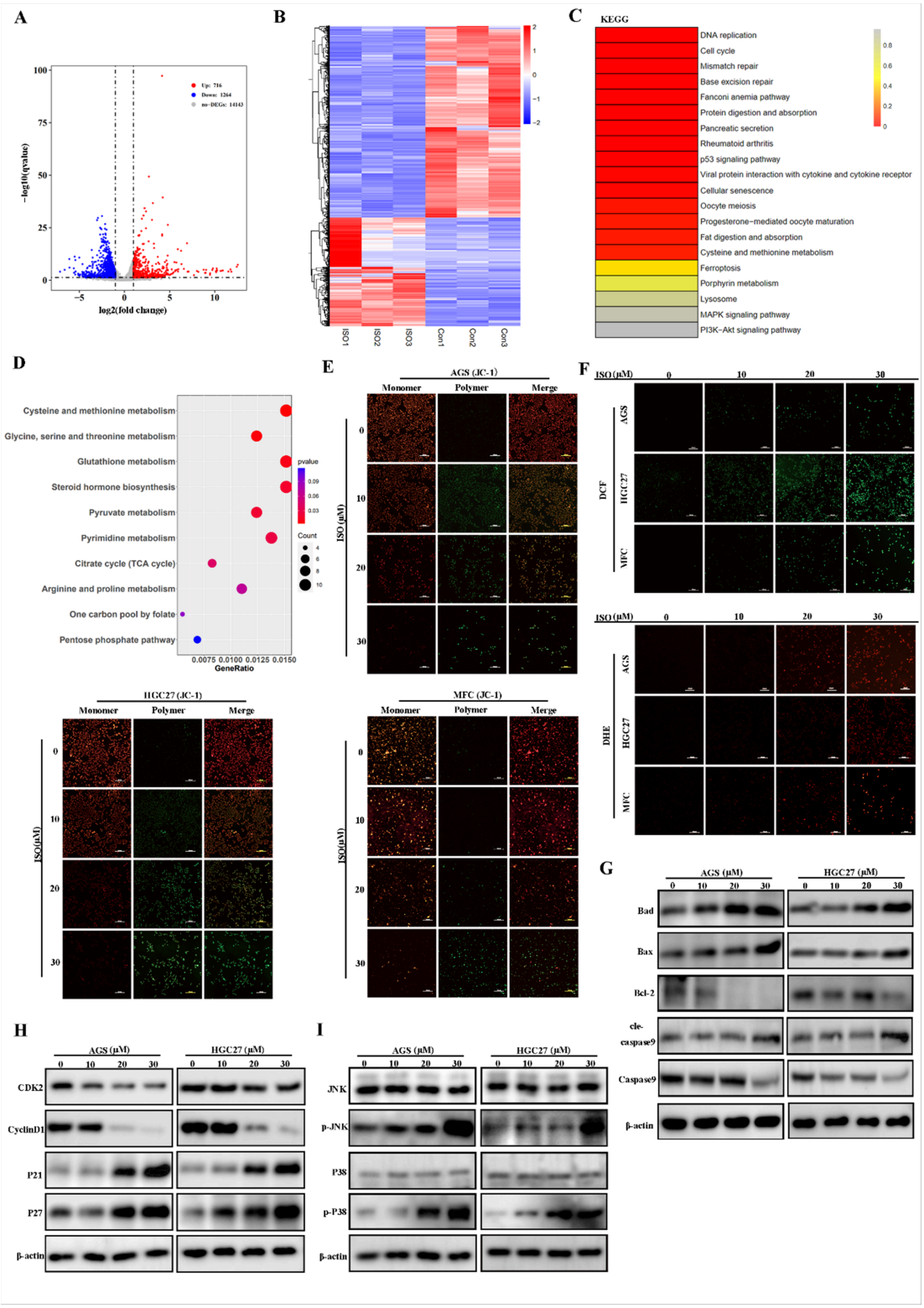


Figure 2

A.AGS cells were treated with 30 μ mol/L ISO for 48 hours. The volcano plot of RNA sequencing revealed significant differentially expressed genes. The screening criteria for differentially expressed genes are | log2 fold change | ≥ 1 and q<0.05. **B.** The RNA sequencing heatmap shows significantly differentially expressed genes. Red represents high gene expression, while blue represents low gene expression. The horizontal axis represents sample clustering, and the vertical axis represents gene clustering. **C.** KEGG

pathway enrichment analysis shows that different colors represent different levels of enrichment, with redder colors indicating more significant enrichment. **D.**GOanalysis showed that differentially expressed genes were significantly enriched in metabolic pathways and TCA cycle. **E.** After treatment with different concentrations of ISO, JC-1 staining was used to evaluate mitochondrial function in cells. **F.** After treatment with different concentrations of ISO, DCF and DHE staining were used to measure oxidative stress levels in cells. **G.** Western blot was used to detect apoptosis-related protein levels in AGS and HGC27 cells after ISO treatment. ISO treatment significantly increased the proportion of cleaved caspase-9/caspase-9, significantly increased Bax and Bad protein levels, and significantly downregulated Bcl-2. **H.** After ISO treatment, Western blot was used to detect CyclinD1, CDK2, P21, and P27 levels in AGS and HGC27 cells. **I.** Western blot was used to detect the protein levels of P-JNK/JNK and P-P38/P38 in the MAPK pathway after ISO treatment. The data is expressed as mean ± standard deviation. Compared with the control group, the significance levels are as follows: * p<0.05, * * p<0.01, * * * p<0.001, * * * * P<0.0001

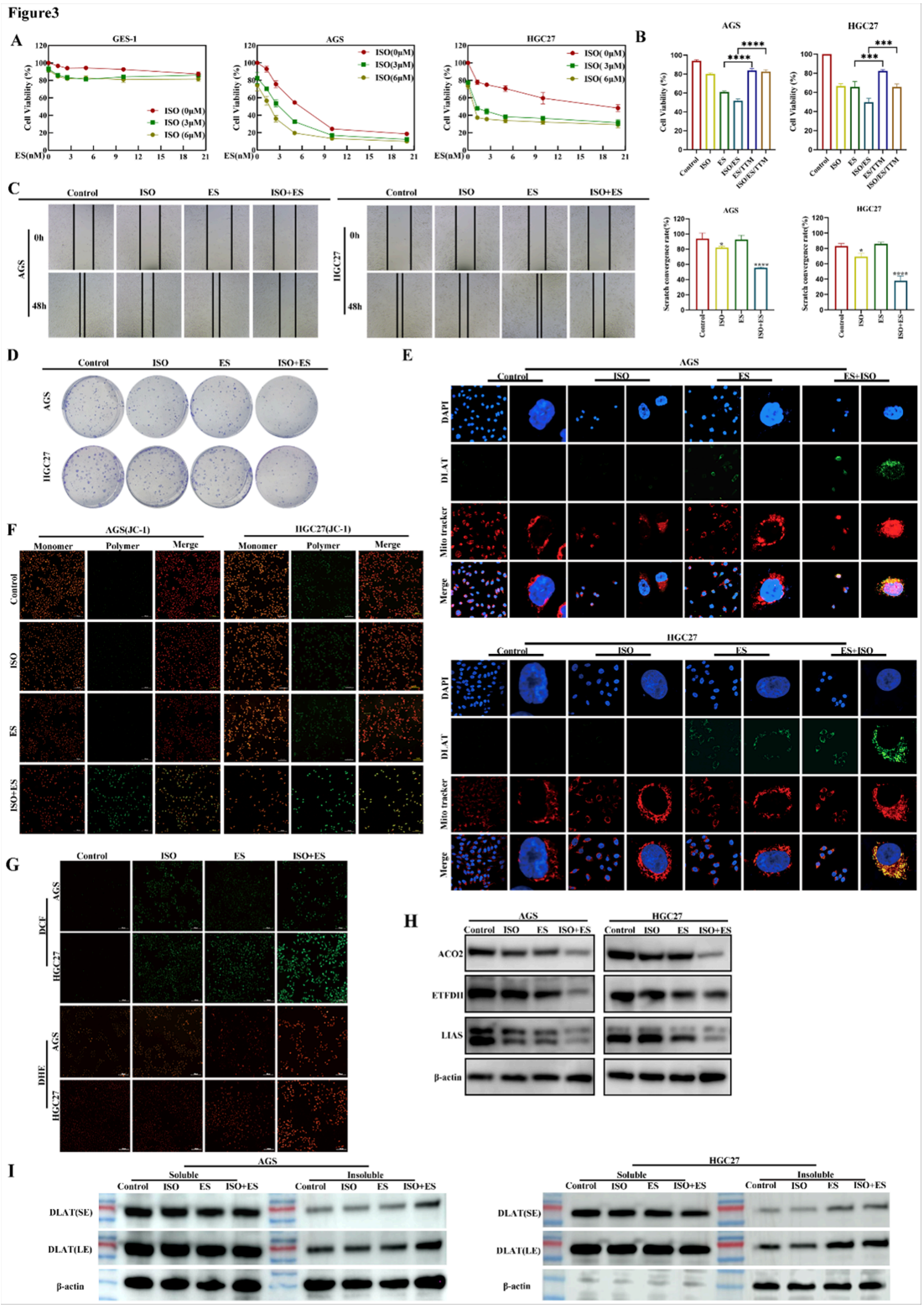


Figure 3

Effects of ISO and ES-Cu, alone and in combination, on gastric cancer cells., **A.** MTT method was used to detect cell viability. **B.** Copper chelator TTM pretreatment and MTT assay for detecting cell viability. **C.** Cell scratch detection of cell migration ability. **D.** Cell cloning detection of cell proliferation ability. **E.** Laser confocal microscopy examination of DLAT oligomerization level. **F.** JC-1 staining to evaluate intracellular mitochondrial function.**G.** DCF and DHE staining were used to measure oxidative stress

levels. **H.** Western blot was used to detect the expression levels of iron sulfur cluster-related proteins ACO2/ETFDH/LIAS. **I.** Western blot was used to detect the expression levels of DLAT in soluble and insoluble proteins. The data is expressed as mean ± standard deviation. Compared with the control group, the significance levels are as follows: * $p<0.05$, * * $p<0.01$, * * * $p<0.001$, * * * * $P<0.0001$

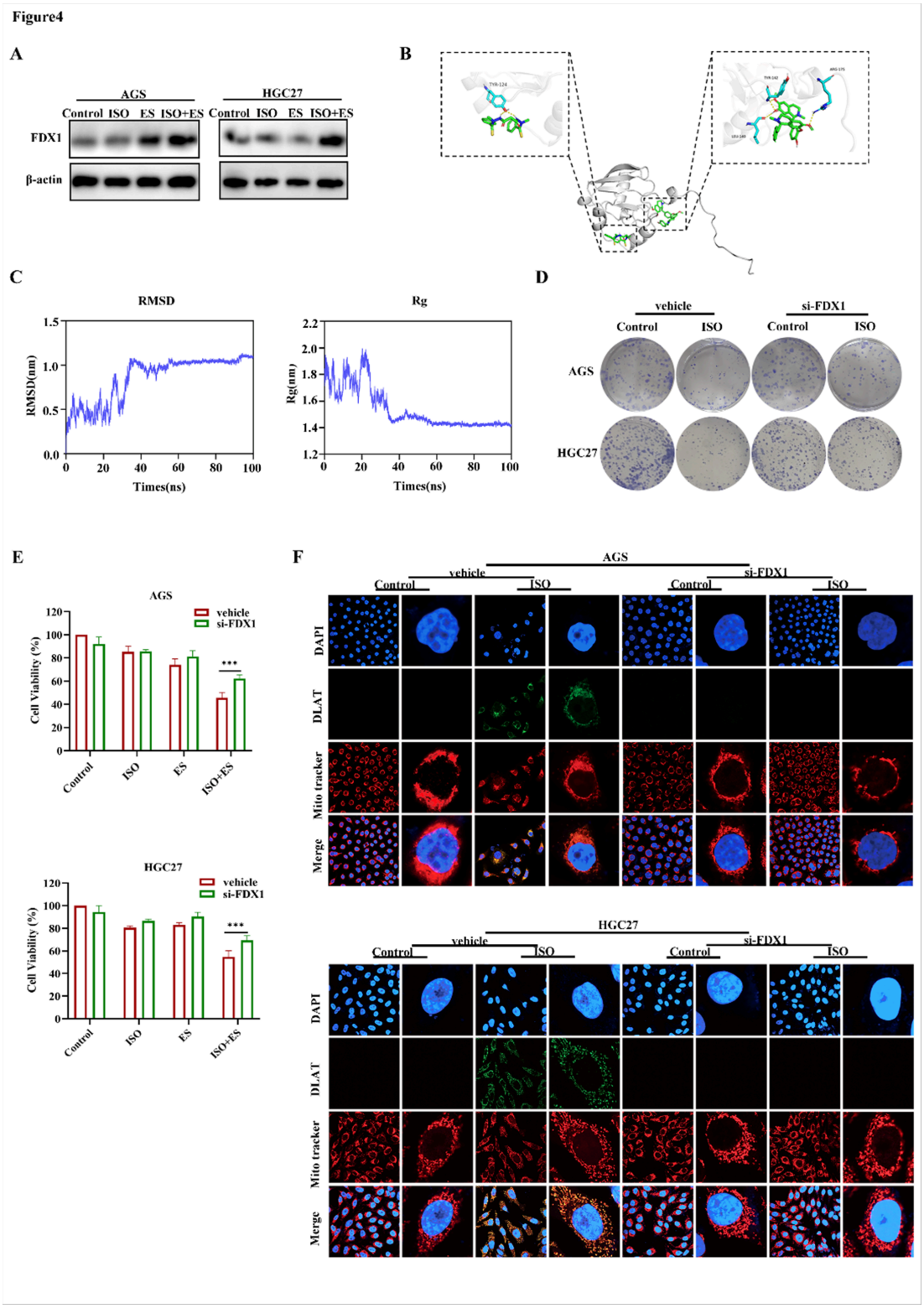


Figure 4

A. Western blot shows significant upregulation of FDX1 protein expression. **B.** Molecular docking mode diagram of ISO combined with ES-Cu and FDX1. **C.**Molecular dynamics simulation diagram of ISO combined with ES-Cu and FDX1. **D.** Cell colony formation ability detected by cell cloning. **E.** Cell viability measured by MTT assay after knocking down FDX1. **F.** Laser confocal measurement of changes in DLAT oligomerization after knocking out FDX1. The data is expressed as mean ± standard deviation. Compared with the control group, the significance levels are as follows: * p<0.05, * * p<0.01, * * * p<0.001, * * * * P<0.0001

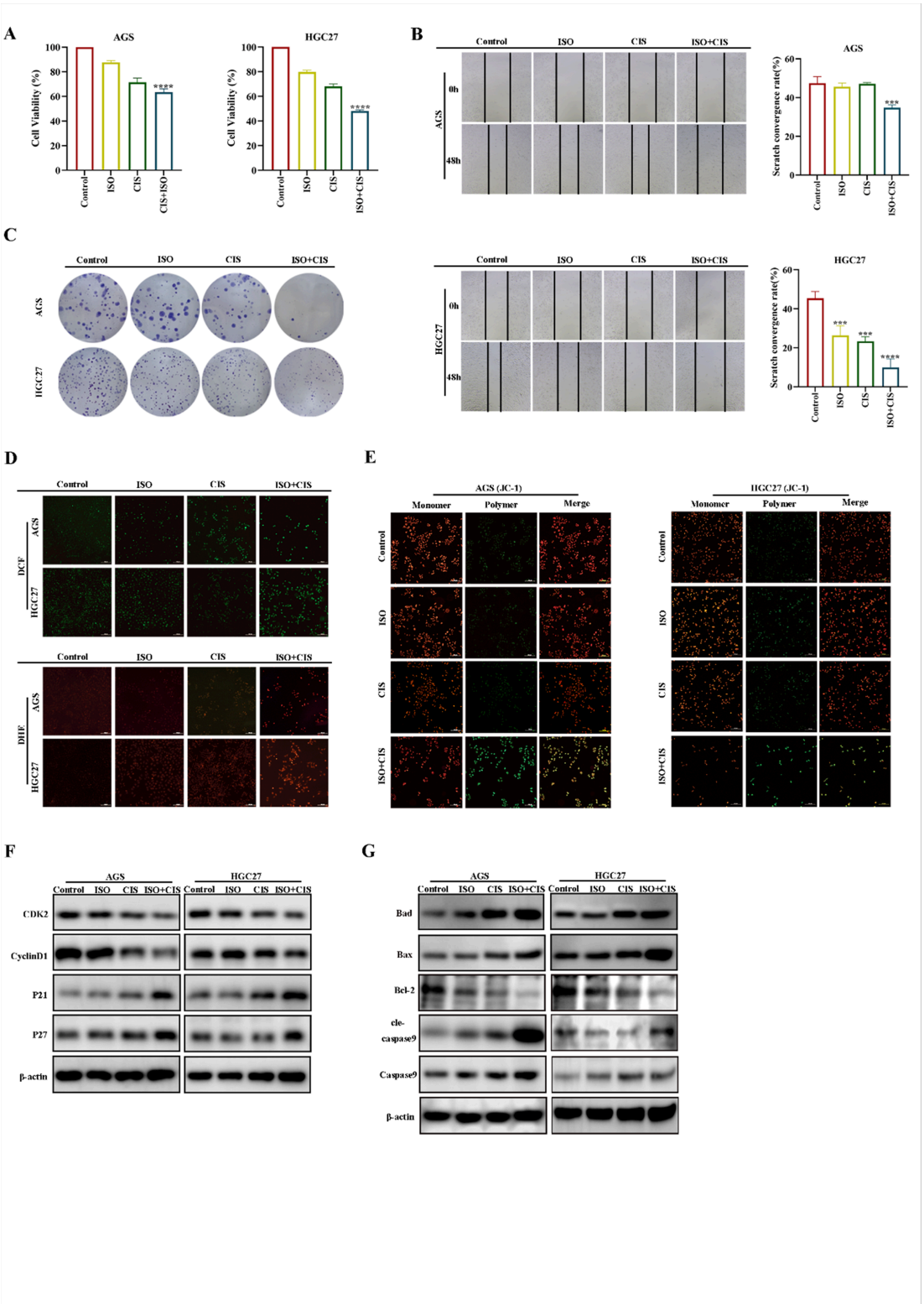


Figure 5

After the combined application of ISO and CIS, the viability of AGS/HGC27 gastric cancer cells was detected by **A.** MTT method. **B.**Cell cloning detection of cell proliferation ability. **C.** Cell scratch detection of cell migration ability. **D.** DCF and DHE staining were used to determine oxidative stress levels. **E.** JC-1 staining was used to evaluate mitochondrial function in cells. **F.**Western blot was used to detect the expression levels of cycle-related proteins CDK2/CyclinD1/P21/P27. **G.** Western blot was used to detect the expression levels of apoptosis-related proteins Bad, Bax, Bcl-2, and cle-caspase9/caspase9. The data is expressed as mean ± standard deviation. Compared with the control group, the significance levels are as follows: * p<0.05, * * p<0.01, * * * p<0.001, * * * * P<0.0001

Supplementary Files

This is a list of supplementary files associated with this preprint. Click to download.

- WB.pdf
- GraphicalAbstract..tif
- GraphicalAbstract..tif